

Non-intrusive detection of methanol in gas phase using infrared degenerate four-wave mixing

J. Zhou¹  · A. L. Sahlberg¹ · H. Nilsson² · E. Lundgren³ · J. Zetterberg¹

Received: 25 June 2015 / Accepted: 20 August 2015 / Published online: 29 August 2015
© Springer-Verlag Berlin Heidelberg 2015

Abstract Sensitive and non-intrusive detection of gas-phase methanol with high spatial and temporal resolution has for the first time been reported using mid-infrared degenerate four-wave mixing (IR-DFWM). IR-DFWM spectra of methanol have been successfully recorded in nitrogen-diluted gas flows at room temperature and at 300 °C, by probing ro-vibrational transitions belonging to the fundamental C–H stretching modes, ν_2 and ν_9 , and the O–H stretching mode, ν_1 . The detection limit of methanol vapor at room temperature and atmospheric pressure is estimated to be 250 ppm with the present setup. Potential interference from CH₄ and CO₂ is discussed from recorded IR-DFWM spectra of CH₄ and CO₂, and it was found that detection of methanol free from CH₄ and CO₂ interference is possible. These results show the potential of the detection of methanol with IR-DFWM for applications in both combustion and catalytic environments, such as CO₂ hydrogenation and CH₄ oxidation.

1 Introduction

Methanol is one of the most important chemicals with industrial applications in a vast variety of areas. It is mainly used as a feedstock in the manufacturing of other

chemicals, including formaldehyde, acetic acid, and olefins, all of which are basic building blocks for a number of common products of modern life. But its use is also increasingly important as a transportation fuel, a fuel cell hydrogen carrier, a source for electricity generation as well as a key component in biodiesel transesterification and wastewater denitrification [1].

The most common method for the production of methanol is to convert feedstock (e.g., natural gas) into syngas (a mixture of carbon monoxide and hydrogen) through gasification process. Syngas can then be converted into methanol through catalytic processes. Direct conversion of CO₂ and CH₄ into methanol through catalytic processes has been a hot topic in both academia and industry over the past decades [2–4]. In such situations, monitoring gas concentrations is necessary to give quantitative information from the processes.

In the operation of direct methanol fuel cells (DMFCs), loss of methanol through gas bubbles at the anode will occur. In this situation, monitoring the concentration of the gas-phase methanol in the exhaust gases will potentially give more valuable quantitative information of the performance of a fuel cell together with the detection of the concentration of the aqueous methanol fed into the fuel cells [5].

Traditionally, Fourier transform infrared spectrometry (FTIR) has been used to detect methanol in the gas phase. Recent work includes measurements of the infrared absorption cross section of methanol at low temperature and pressure (204.5 K and 50.92 Torr) with high resolution [6], and at atmospheric pressure and elevated temperatures (up to 778 K) [7], but with lower resolution. However, FTIR is a line-of-sight technique, which cannot provide spatial resolution along the light-propagating axis, introducing distortions in the spectral features due to species and temperature

✉ J. Zhou
Jianfeng.zhou@forbrf.lth.se

¹ Division of Combustion Physics, Lund University, 221 00 Lund, Sweden

² Department of Astronomy and Theoretical Physics, Lund University, 221 00 Lund, Sweden

³ Division of Synchrotron Radiation Research, Lund University, 221 00 Lund, Sweden

variations along the propagating path, and its temporal resolution is limited by the integration time (typically on the order of seconds or more). Recent developments of cavity-enhanced absorption spectroscopy with quantum cascade lasers can provide detection of infrared active species with millisecond resolution [8]. However, it is a technique based on multi-path absorption and cannot provide high spatial resolution. In several applications, such as catalysis, monitoring methanol non-intrusively is very attractive and would contribute to better understanding when characterizing catalysts in the catalytic processes. This calls for a method to provide in situ detection of methanol with both high temporal and spatial resolution.

Degenerate four-wave mixing (DFWM) is a nonlinear optical technique that can provide high temporal and spatial resolution. The theory of DFWM was first presented by Abrams and Lind in 1978 [9, 10]. This study assumed the phase-conjugate geometry and a weak probe beam compared to the pump beams. The theory of DFWM has been extensively treated afterward, both numerically and analytically [11, 12]. The first application for the detection of flame species was performed by Ewart et al. [13] for the detection of the OH radical. Since then, DFWM with UV–Visible lasers has been widely applied in combustion diagnostics for the detection of molecules and radicals [14–17]. The theory and applications of DFWM were recently reviewed by Kiefer and Ewart [18].

Compared to UV–Visible DFWM, mid-infrared DFWM (IR-DFWM) has been less widely applied, in part due to the lack of suitable lasers and detectors in this spectral region. Advances in the field of lasers and infrared detectors have made IR-DFWM an attractive laser technique for the detection of molecules that lack accessible transitions in the UV–Visible range, such as HF [19], HCl [20], CH₄ [21, 22], and C₂H₂ [21, 23]. Sun et al. recently reported the design of infrared BOXCAR plates for stable alignment of IR-DFWM in the forward phase-matching geometry for the detection of C₂H₂ and HCl [24]. A similar setup was used by Sahlberg et al. [25] for the detection of CH₃Cl in hot gas flows. These studies prove the potential of IR-DFWM as

a powerful spectroscopic tool for sensitive in situ spectroscopic measurements of infrared active species with high spatial and temporal resolution.

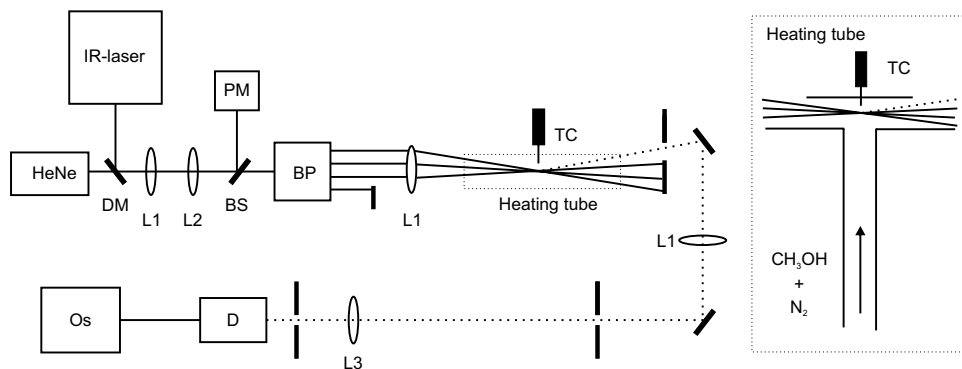
Methanol has four fundamental vibrational modes in the mid-infrared spectral region that can be probed using IR-DFWM: the ν_1 O–H stretching near 3681 cm⁻¹, the ν_2 C–H asymmetric stretching (A') near 3000 cm⁻¹, the ν_9 C–H asymmetric stretching (A'') near 2970 cm⁻¹, and the ν_3 C–H parallel symmetric stretch (A') near 2844 cm⁻¹. Studies and modeling of the C–H stretching region of methanol can be found in a number of works [26–29].

In this study, the ν_2 and ν_9 C–H stretching in the frequency range from 2960 to 3030 cm⁻¹ and the ν_1 O–H stretching in the frequency range from 3650 to 3700 cm⁻¹ were probed using IR-DFWM, and measurements were taken both at room temperature and at 300 °C and compared to simulated absorption spectra. Trace concentrations of CH₄ and CO₂ were separately seeded into the methanol gas flow, and the position of the CH₄ and CO₂ spectral lines was used for wavelength calibration, as well as for demonstrating that methanol detection with IR-DFWM can be made free from interference of CH₄ and CO₂.

2 Experiment

A schematic of the IR-DFWM setup is shown in Fig. 1. The laser system for the generation of mid-infrared light has been described previously [30], and only a brief account will be given here. The second harmonic of an injection seeded Nd:YAG laser (Spectra Physics, PRO 290-10) at 532 nm was used to pump a dye laser system (Sirah, PRSC-D-18) running on LDS 798 and LDS 765 dye (Exiton), with ethanol as solvent, which gives tunable pulsed laser radiation over a broad wavelength range 758–826 and 738–800 nm, respectively. The dye laser light was then difference frequency mixed in a LiNbO₃ crystal together with the residual fundamental 1064-nm laser light from the Nd:YAG laser, generating mid-infrared laser pulses. The mid-infrared laser light was further amplified in another

Fig. 1 Schematic of the experimental setup. *BP* BOXCAR plates, *TC* thermocouple, *DM* dichroic mirror, *BS* beam splitter (CaF₂ window) *L1* CaF₂ lens, $f = 300$ mm, *L2* CaF₂ lens, $f = -200$ mm, *L3* CaF₂ lens, $f = 100$ mm, *D* InSb detector, *Os* oscilloscope, *PM* power meter



LiNbO₃ crystal pumped by 1064-nm light. This process generates tunable mid-infrared laser light with 10-Hz repetition rate, ~4-ns pulse length with a pulse energy of ~3 mJ and a linewidth of 0.025 cm⁻¹ [31]. A telescope was used to shrink the beam size down to approximately 3 mm. The reflection from a CaF₂ window was sent to a power meter to monitor the laser energy during the scan. The mid-IR beam was overlapped with a He–Ne laser beam to facilitate the alignment. The laser wavelength was scanned over the wavelength of the absorption peaks by tuning the dye laser wavelength.

The laser beam was split into four parallel beams using a set of IR-BOXCAR plates, which have been described elsewhere [24]. Three of the parallel laser beams were crossed using an $f = 300$ mm CaF₂ focusing lens, and the IR-DFWM signal is generated in the crossing point of the three beams. The probe volume in this setup was estimated to be $0.4 \times 0.4 \times 6$ mm³. The signal will follow the path of the fourth laser beam; thus, this beam was used to trace the signal to the detector. The signal beam was collimated using another $f = 300$ mm CaF₂ lens and focused onto an InSb liquid-nitrogen-cooled photodetector (Judson technologies, J10D-M204-R04 M-60). A number of apertures were used to block background scattering, and the signal from the detector was logged by a digital oscilloscope (LeCroy Waverunner 6K).

Methanol vapor was prepared using a bubbler, which was bathed in ice water to keep the temperature of the bubbler at 0 °C, ensuring no condensation will occur along the way to the measurement region. Carrier flow (N₂) entering into bubbler was kept below 2 l/min to make sure that the mole fraction of methanol vapor is stabilized. The gas flows were controlled by Bronkhorst mass flow controllers, and the concentration of methanol was adjusted by diluting the flow from the bubbler with a second N₂ flow. When used, CH₄ or CO₂ was also mixed into the flow after the bubbler. The gas flows were directed to an open T-shaped gas tube as illustrated in Fig. 1. The total flow of the gases through the tube was kept around 4.5 l/min, giving a flow speed at room temperature of about 25 cm/s at the measurement point.

The heating gas tube is made of fused silica glass and surrounded by an electric heating wire and insulation. A thermocouple was inserted through the top of the gas tube, to monitor the gas temperature. The temperature in the crossing point of the laser beams was assumed to be uniform and to be the same as that which the thermocouple measured.

To measure the concentrations of methanol vapor prepared by the method described above, an absorption spectrum of methanol was recorded with the Lund Observatory Bruker IFS 125 HR Fourier transform spectrometer. The maximum resolution of the instrument is 0.0021 cm⁻¹,

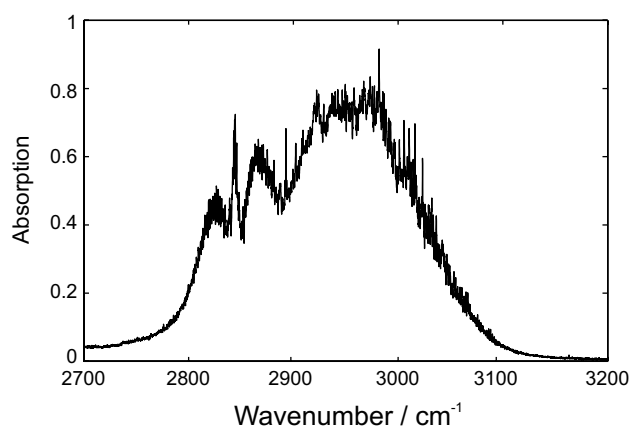


Fig. 2 An FTIR absorption measurement of methanol vapor in a 10-cm-long gas cell at room temperature and atmospheric pressure

which is achieved by using the full optical path difference of 4.3 m. However, the resolution used to resolve the methanol spectrum was 0.1 cm⁻¹. A total of 200 scans were co-added in order to achieve a high signal-to-noise ratio. The spectrum was recorded from a 10-cm-long gas cell illuminated by a continuous tungsten ribbon lamp with known relative intensity distribution.

3 Measurements and results

An FTIR absorption spectrum of methanol vapor at room temperature and atmospheric pressure in a 10-cm gas cell is shown in Fig. 2. By using the Beer–Lambert law in Eq. (1),

$$1 - \alpha_v = \exp\left(-\frac{qPx}{kT}\sigma_v\right) \quad (1)$$

where α_v is the absorptivity, σ_v is the IR cross section, q is concentration, P is the pressure, T is the temperature, k is Boltzmann's constant, and x is the path length; the concentration of methanol at a vapor pressure of 0 °C is calculated to be 4 %. With this known concentration, the methanol vapor was further diluted with N₂ for quantitative studies in the following.

To investigate the ν_2 and ν_9 modes of methanol, IR-DFWM spectra were recorded and compared to simulated absorption spectrum, based on the IR cross section of methanol from the NIST IR database [32]. Figure 3a shows a simulated absorption spectrum of 3200 ppm methanol at room temperature and atmospheric pressure, for a path length of 10 cm. Two IR-DFWM scans were recorded, one in a gas flow of 3200 ppm methanol in nitrogen at room temperature and one in a gas flow of 8300 ppm methanol in nitrogen at 300 °C, shown in Fig. 3b, c respectively.

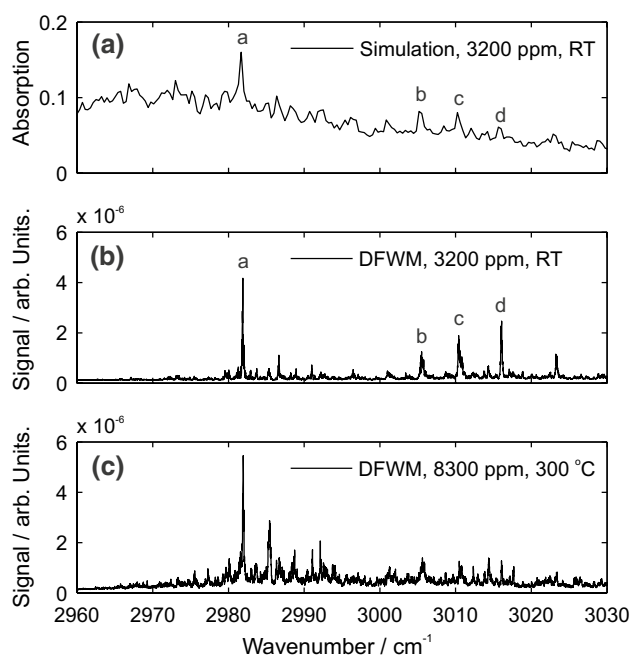


Fig. 3 A comparison between a simulated absorption spectrum and the measured IR-DFWM spectrum for the ν_2 and ν_9 modes of methanol. **a** A simulated absorption spectrum of 3200 ppm methanol at room temperature, atmospheric pressure, and for a path length of 10 cm. **b** A measured IR-DFWM spectrum of 3200 ppm methanol at room temperature. **c** A measured IR-DFWM spectrum of 8300 ppm methanol at 300 °C. Transitions for Q-branches in features *a–d* are shown in Table 1

Due to the large amplitude of the internal rotation and the small amplitude vibrations, the vibrational spectra in the infrared are highly congested at room temperature [28]. Therefore, the simulated absorption spectrum exhibits a very broad feature. Interestingly, compared to the absorption spectrum, the IR-DFWM spectrum in panel (b) shows a highly enhanced signal for the features labeled *a–d*. These features cannot be resolved in the IR-DFWM spectra, but can be identified as Q-branches following the work of Xu et al. [28]. As listed in Table 1, feature *a* consists of two *A* symmetry Q-branches: $K = 2 \leftarrow 3$ and $K = 1 \leftarrow 2$; feature *b* consists of one *E* symmetry Q-branch $K = 2 \leftarrow 1$ and one *A* symmetry Q-branch $K = 2 \leftarrow 1$; feature *c* consists of one *A* symmetry Q-branch $K = 3 \leftarrow 2$; and feature *d* consists of one *E* symmetry Q-branch $K = -3 \leftarrow -2$. Each of these Q-branches contains a number of closely spaced transitions, resulting in a coherent enhancement of the IR-DFWM signal, making the spectral feature more distinct. A similar phenomenon has been observed in the IR-DFWM spectra of CH_3Cl [25]. There have been studies of the interaction of closely spaced spectral lines in DFWM [33–35], showing that closely spaced lines can constructively interfere to produce a stronger signal. Those studies also suggest that destructive interference might also occur depending on the absolute line positions and laser power and detuning. This, however, was not observed in this study, which might be also due to the fact that the phase-conjugate geometry is

Table 1 *A* and *E* symmetry transitions (in cm^{-1}) for the selected methanol features in Fig. 3

Feature	a		b		c	d
	<i>A</i>	<i>A</i>	<i>E</i>	<i>A</i>		
Q-branch	$K = 2 \leftarrow 3$	$K = 1 \leftarrow 2$	$K = 2 \leftarrow 1$	$K = 2 \leftarrow 1$	$K = 3 \leftarrow 2$	$K = -3 \leftarrow -2$
Transitions wave number (cm^{-1})	2981.8084	2982.4590	3005.4221	3006.2705	3010.3242	3016.0252
	2981.8146	2982.5005	3005.4312	3006.2334	3010.3384	3016.0356
	2981.8147	2982.5554	3005.4426	3006.1848	3010.3574	3016.0483
		2982.6235	3005.4575	3006.1257	3010.3838	3016.0630
		2982.7046	3005.4751	3006.0576	3010.4126	3016.0784
		2982.7966	3005.4945	3006.9783	3010.3782	
		2982.3909	3005.5134	3006.8933	3010.4053	
		2982.3648		3006.8010		
		2982.3298		3006.3538		
		2982.2864		3006.3992		
		2982.2351		3006.4602		
		2982.1751		3006.5359		
				3006.6277		
				3006.7324		
				3006.8543		

Data extracted from Ref. [28]

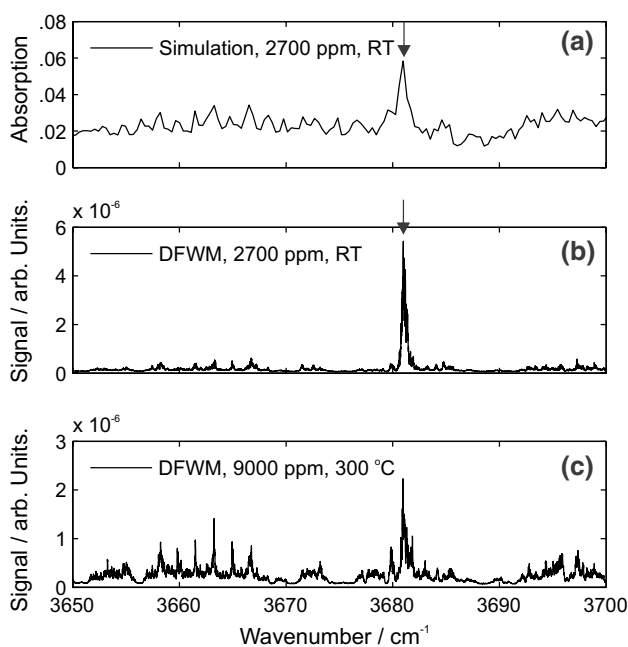


Fig. 4 A comparison between the simulated absorption spectrum and the measured IR-DFWM spectra in the ν_1 band of methanol. The arrow indicates the Q-branch feature near 3681 cm^{-1} . **a** A simulated absorption spectrum of 2700 ppm methanol at room temperature and atmospheric pressure with a path length of 10 cm. **b** A measured IR-DFWM spectrum of 2700 ppm methanol at room temperature. **c** A measured IR-DFWM spectrum of 9000 ppm methanol at $300\text{ }^\circ\text{C}$

assumed in those studies, as opposed to the forward phase-matching geometry investigated in this work. In panel (c), a continuous background-like signal arises at higher temperature, which is due to many upper vibrational levels of methanol molecules are further populated. The Q-branch feature near 2982 cm^{-1} is, however, very easy to identify. Therefore, this feature will be focused on in the discussion later.

A similar investigation was performed for the ν_1 mode of methanol. A simulated absorption spectrum of 2700 ppm methanol at room temperature and atmospheric pressure with a path length of 10 cm is shown in Fig. 4a. Two IR-DFWM scans were recorded, one in a gas flow of 2700 ppm of methanol in nitrogen at room temperature and one in a gas flow of 9000 ppm of methanol in nitrogen at $300\text{ }^\circ\text{C}$, respectively, shown in Fig. 4b, c. According to the work of Kleiner et al. [36], the unresolved feature marked with an arrow near 3681 cm^{-1} consists of two Q-branches: $E: J_{-1} \leftarrow J_0$ and $E: J_{+1} \leftarrow J_{+2}$. Each of these Q-branches contains many closely spaced transitions. Therefore, following the same argument, enhancement of the signal for this feature in the IR-DFWM spectra can also be seen.

As water vapor in the ambient air is a strong absorber in the mid-infrared spectral region, spectral lines that are not overlapping with strong water absorption lines need to

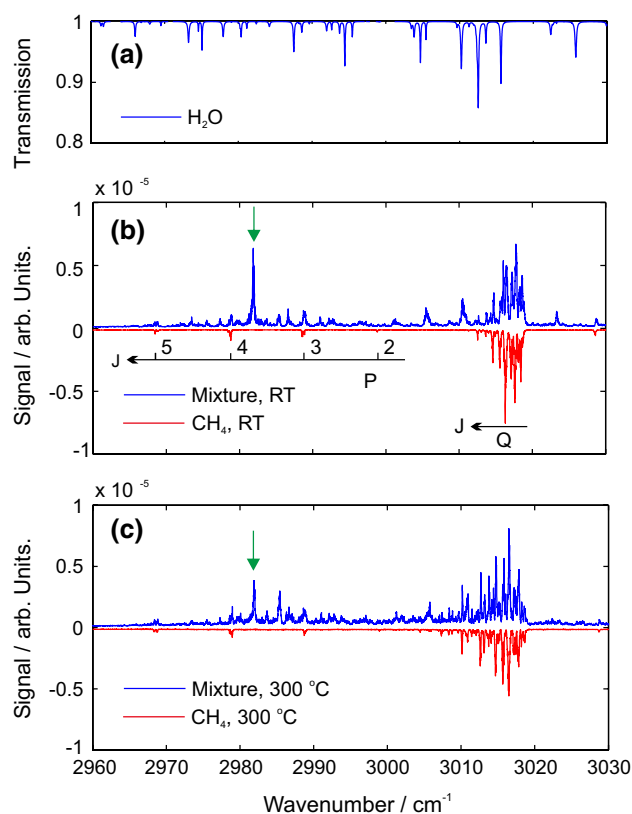


Fig. 5 Illustration of the CH_4 interference around 3000 cm^{-1} . **a** A simulated transmission spectrum of 0.5 % H_2O vapor in the ambient air and a path length of 3 m. **b** A measured IR-DFWM spectrum (in blue) in a mixture of 3200 ppm methanol and 250 ppm CH_4 gas flow, and a measured IR-DFWM spectrum (in red) in 270 ppm CH_4 gas flow at room temperature. Partial assignments for CH_4 lines have been made. **c** A measured IR-DFWM spectrum (in blue) in a mixture of 8300 ppm methanol and 850 ppm CH_4 gas flow, and a measured IR-DFWM spectrum (in red) in 800 ppm CH_4 gas flow at $300\text{ }^\circ\text{C}$. The green arrow indicates the Q-branch feature of methanol near 2982 cm^{-1}

be chosen when detecting methanol. A simulated transmission spectrum, based on molecular parameters extracted from the HITRAN database [37], with 0.5 % H_2O vapor in the ambient air and with a path length of 3 m (simulating the present setup), is shown in Fig. 5a. It can be seen that laser attenuation by H_2O absorption is negligible in the selected frequency range. Another species that could potentially interfere with methanol in several applications is CH_4 . To illustrate that potential interference around 3000 cm^{-1} , a trace concentration of CH_4 was seeded into the methanol–nitrogen flow, preparing a mixture of methanol and CH_4 , which were then further diluted in a nitrogen flow. Figure 5b shows an IR-DFWM spectrum (in blue) from a mixture of 3200 ppm methanol and 250 ppm CH_4 in nitrogen, and an IR-DFWM spectrum (in red) of 270 ppm CH_4 in nitrogen at room temperature. Figure 5c shows an IR-DFWM spectrum (in blue) in a mixture of 8300 ppm

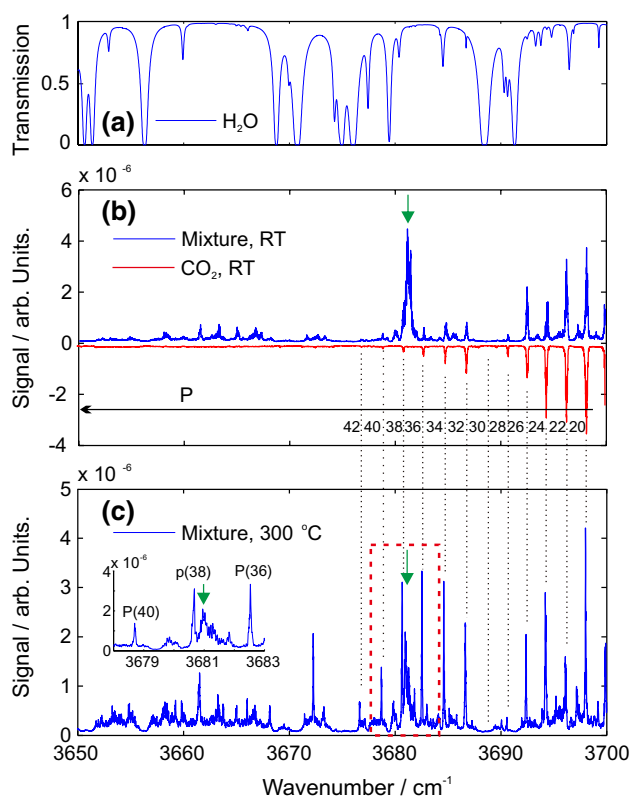


Fig. 6 Illustration of the CO_2 interference around 3680 cm^{-1} . **a** A simulated transmission spectrum of 0.5 % H_2O vapor in the ambient air and a path length of 3 m. **b** A measured IR-DFWM spectrum (in blue) in a mixture of 2700 ppm methanol and 1300 ppm CO_2 gas flow, and a measured IR-DFWM spectrum (in red) in 1300 ppm CO_2 gas flow at room temperature. Partial assignments for CO_2 lines have been made. **c** A measured IR-DFWM spectrum in a mixture of 8800 ppm methanol and 2100 ppm CO_2 gas flow at $300\text{ }^\circ\text{C}$. A zoom of part of the spectrum (marked by the red dashed box) is shown in the inset. The green arrow indicates the Q-branch feature of methanol near 3681 cm^{-1}

methanol and 850 ppm CH_4 in nitrogen, and an IR-DFWM spectrum (in red) of 800 ppm CH_4 in nitrogen at $300\text{ }^\circ\text{C}$. Hot CH_4 lines in the Q-branch can be identified by comparing the CH_4 spectra in Fig. 5b, c. It can be clearly seen that both at room temperature and at $300\text{ }^\circ\text{C}$, the methanol feature near 2982 cm^{-1} (marked by the green arrow) is free from CH_4 interference.

In the same manner as the previous section, water vapor absorption in the ambient air was studied to investigate the suitability of detecting methanol by its ν_1 band. Figure 6a shows a simulated transmission spectrum of 0.5 % H_2O vapor in the ambient air with a path length of 3 m. As can be seen, absorption due to water vapor is much more pronounced in this frequency range. Interference from CO_2 should also be considered when

detecting methanol in combustion environments, since CO_2 is one of the most common product gases in combustion. To demonstrate the interference from CO_2 around 3680 cm^{-1} , a trace concentration of CO_2 was seeded into the methanol flow, preparing a mixture of methanol and CO_2 at trace concentration in the nitrogen flow. Figure 6b shows an IR-DFWM spectrum (in blue) acquired in a mixture of 2700 ppm methanol and 1300 ppm CO_2 gas flow, and an IR-DFWM spectrum (in red) in 1300 ppm CO_2 gas flow, both diluted in nitrogen and at room temperature. Figure 6c shows an IR-DFWM spectrum in a mixture of 8800 ppm methanol and 2100 ppm CO_2 diluted in nitrogen at $300\text{ }^\circ\text{C}$. An inset in Fig. 6c zooms in on the region where the methanol feature near 3681 cm^{-1} , marked by a green arrow, is close to the P(38) line of CO_2 . Even though these two lines are partly overlapped in the wings, detection of methanol is free from CO_2 interference. It can be seen that the missing of P(30) line of CO_2 is due to strong laser attenuation by absorption from water vapor in the ambient air. However, detection of the methanol line near 3681 cm^{-1} is still feasible due to significantly lower H_2O absorption in the range from 3680 to 3682 cm^{-1} .

The dependency of the IR-DFWM signal on methanol number densities was investigated to demonstrate the quantitative ability of IR-DFWM. Figure 7 shows the line-integrated IR-DFWM signal intensities collected at different methanol concentrations at room temperature, by scanning over the Q-branch features near 2982 and 3681 cm^{-1} , respectively. The line-integrated IR-DFWM signals of three repeated scans were averaged for each concentration, and the error bars show the standard deviation. The line-integrated DFWM signal is expected to have a quadratic dependence on the concentration of the absorbed species under optically thin conditions [18]. Therefore, a quadratic function $S = a \cdot X^2$ was adopted to fit the signal-concentration curve, with which a satisfactory fitting was obtained. The small deviation from the quadratic fitting can be attributed to the self-absorption of the signal inside the tube, and the fact that the scanned methanol features contain many closely spaced transitions instead of only one transition which is assumed in the model. Based on the signal-to-noise ratio, detection limits were estimated to be approximately 350 and 250 ppm by detecting the Q-branch features near 2982 and 3681 cm^{-1} , respectively. The insets in Fig. 7 show the raw signals at 500 and 690 ppm methanol concentrations accordingly and illustrate the high signal levels obtained at these relatively low concentrations. The underlying regular pattern of fringes in the raw IR-DFWM signal is from periodic variations in the laser energy due to etalon effect in the dye laser during scanning.

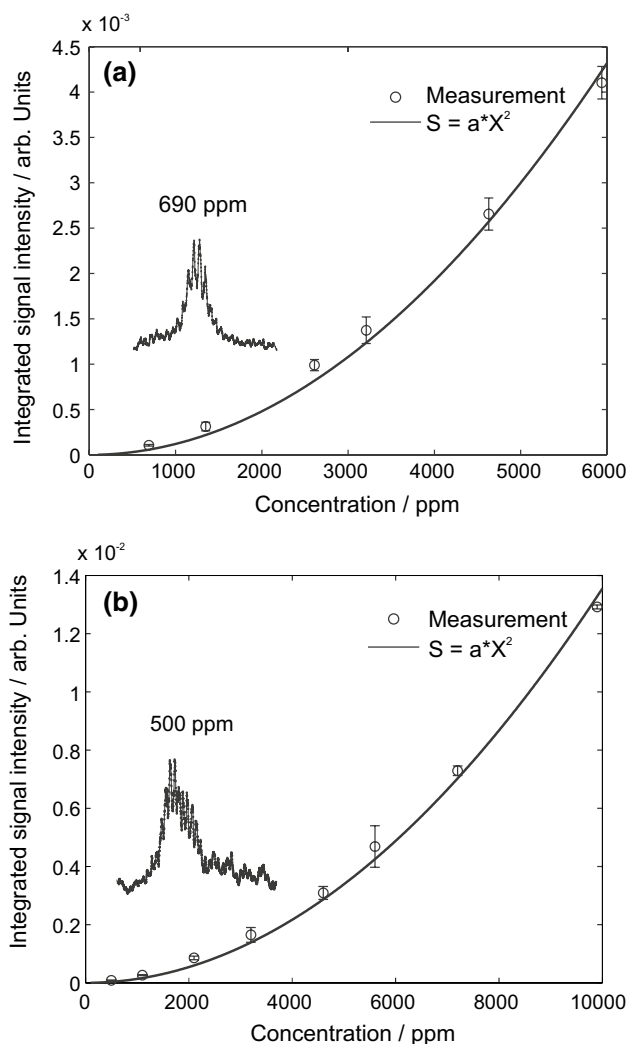


Fig. 7 Dependency of the IR-DFWM signal on methanol concentration by scanning over the Q-branch features near 2982 cm^{-1} (a) and 3681 cm^{-1} (b). The insets of a, b show the IR-DFWM signal at 690 ppm and 500 ppm, respectively. A quadratic function is used to fit the signal–concentration curve

4 Conclusions

In this work, we have demonstrated the potential of IR-DFWM as an in situ tool for sensitive and non-intrusive detection of gas-phase methanol with a spatial resolution of about $0.4 \times 0.4 \times 6\text{ mm}^3$ and a temporal resolution of about 4 ns. This makes IR-DFWM an attractive candidate for the detection of gas-phase methanol. Traditional FTIR methods, often used for methanol detection, have limited spatial and temporal resolution, something the presented IR-DFWM technique can deliver and makes it a good complement for the detection of gas-phase methanol.

Owing to the coherent enhancement of the IR-DFWM signal from many closely spaced transitions in the

Q-branches of methanol, the IR-DFWM spectra show much enhanced signal for the Q-branch features, making the spectra much more distinct than the absorption spectra. At the same time, the line-integrated IR-DFWM signal still shows a simple quadratic dependence on the methanol number density to a satisfactory degree, simplifying the quantitative analysis significantly.

Two interference-free detection schemes (by detecting Q-branch features near 2982 and 3681 cm^{-1}) have been proposed. Laser attenuation by water vapor absorption in the ambient air has been shown theoretically to be insignificant. Both detection schemes can achieve detection limits down to hundreds of ppm at room temperature and atmospheric pressure. When the Q-branch feature near 2982 cm^{-1} is used, its close proximity to the P(4) line of CH_4 provides the possibility of combined detection of methanol and CH_4 . Similarly, when the Q-branch feature near 3681 cm^{-1} is used, its close proximity to P(38) line of CO_2 gives the possibility of combined detection of methanol and CO_2 . This can be very useful when detecting methanol in catalytic reactions, e.g., CO_2 hydrogenation and CH_4 oxidation.

Acknowledgments This work was financially supported by the Knut and Alice Wallenberg Foundation and the Carl Trygger Foundation for Scientific Research.

References

1. <http://www.methanol.org/>. Accessed May 2015
2. I. Ganesh, *Renew. Sustain. Energy Rev.* **31**, 221 (2014)
3. W. Wang, S.P. Wang, X.B. Ma, J.L. Gong, *Chem. Soc. Rev.* **40**, 3703 (2011)
4. Y.M. Chen, D.E. Clemmer, P.B. Armentrout, *J. Am. Chem. Soc.* **116**, 7815 (1994)
5. M.Z. Florian, J.B. Euan, K. Johannes, *Meas. Sci. Technol.* **23**, 045602 (2012)
6. J.J. Harrison, N.D.C. Allen, P.F. Bernath, *J. Quant. Spectrosc. Radiat. Transfer* **113**, 2189 (2012)
7. M. Alrefae, E.T. Es-sebbar, A. Farooq, *J. Mol. Spectrosc.* **303**, 8 (2014)
8. G. Maisons, P.G. Carbajo, M. Carras, D. Romanini, *Opt. Lett.* **35**, 3607 (2010)
9. R.L. Abrams, R.C. Lind, *Opt. Lett.* **2**, 94 (1978)
10. R.L. Abrams, R.C. Lind, *Opt. Lett.* **3**, 205 (1978)
11. T.A. Reichardt, R.P. Lucht, P.M. Danehy, R.L. Farrow, *J. Opt. Soc. Am. B Opt. Phys.* **15**, 2566 (1998)
12. R.T. Bratfalean, G.M. Lloyd, P. Ewart, *J. Opt. Soc. Am. B Opt. Phys.* **16**, 952 (1999)
13. P. Ewart, S.V. O'leary, *Opt. Lett.* **11**, 279 (1986)
14. P. Ewart, P. Snowdon, *Opt. Lett.* **15**, 1403 (1990)
15. R.L. Farrow, D.J. Rakestraw, *Science* **257**, 1894 (1992)
16. K. Kohseinghaus, *Prog. Energy Combust. Sci.* **20**, 203 (1994)
17. A.C. Eckbreth, *Laser Diagnostics for Combustion Temperature and Species* (Gordon and Breach, Amsterdam, 1996)
18. J. Kiefer, P. Ewart, *Prog. Energy Combust. Sci.* **37**, 525 (2011)
19. R.L. Vanderwal, B.E. Holmes, J.B. Jeffries, P.M. Danehy, R.L. Farrow, D.J. Rakestraw, *Chem. Phys. Lett.* **191**, 251 (1992)

20. G.J. Germann, D.J. Rakestraw, *Science* **264**, 1750 (1994)
21. G.J. Germann, R.L. Farrow, D.J. Rakestraw, *J. Opt. Soc. Am. B Opt. Phys.* **12**, 25 (1995)
22. K. Richard, P. Ewart, *Appl. Phys. B Lasers Opt.* **94**, 715 (2009)
23. Y. Tang, S.A. Reid, *Chem. Phys. Lett.* **248**, 476 (1996)
24. Z.W. Sun, Z.S. Li, B. Li, M. Alden, P. Ewart, *Appl. Phys. B Lasers Opt.* **98**, 593 (2010)
25. A.L. Sahlberg, J. Zhou, M. Aldén, Z.S. Li, *J. Raman. Spectrosc.* **46**, 695 (2015)
26. R.H. Hunt, W.N. Shelton, W.B. Cook, O.N. Bignall, J.W. Mirick, F.A. Flaherty, *J. Mol. Spectrosc.* **149**, 252 (1991)
27. O.N. Bignall, R.H. Hunt, W.N. Shelton, *J. Mol. Spectrosc.* **166**, 137 (1994)
28. L.H. Xu, X. Wang, T.J. Cronin, D.S. Perry, G.T. Fraser, A.S. Pine, *J. Mol. Spectrosc.* **185**, 158 (1997)
29. G.L. Villanueva, M.A. DiSanti, M.J. Mumma, L.H. Xu, *Astrophys. J.* **747**, 37 (2012)
30. Z.T. Alwahabi, J. Zetterberg, Z.S. Li, M. Alden, *Eur. Phys. J. D* **42**, 41 (2007)
31. Z.S. Li, M. Rupinski, J. Zetterberg, Z.T. Alwahabi, M. Alden, *Chem. Phys. Lett.* **407**, 243 (2005)
32. P.M. Chu, F.R. Guenther, G.C. Rhoderick, W.J. Lafferty, *Quantitative Infrared Database* (National Institute of Standards and Technology, Gaithersburg, 1999), p. 20899
33. T.A. Reichardt, R.P. Lucht, *J. Opt. Soc. Am. B Opt. Phys.* **14**, 2449 (1997)
34. C.F. Kaminski, I.G. Hughes, P. Ewart, *J. Chem. Phys.* **106**, 5324 (1997)
35. G.M. Lloyd, P. Ewart, *J. Chem. Phys.* **110**, 385 (1999)
36. I. Kleiner, G.T. Fraser, J.T. Hougen, A.S. Pine, *J. Mol. Spectrosc.* **147**, 155 (1991)
37. L.S. Rothman, I.E. Gordon, A. Barbe, D.C. Benner, P.E. Bernath, M. Birk, V. Boudon, L.R. Brown, A. Campargue, J.P. Champion, K. Chance, L.H. Coudert, V. Dana, V.M. Devi, S. Fally, J.M. Flaud, R.R. Gamache, A. Goldman, D. Jacquemart, I. Kleiner, N. Lacombe, W.J. Lafferty, J.Y. Mandin, S.T. Massie, S.N. Mikhailenko, C.E. Miller, N. Moazzen-Ahmadi, O.V. Naumenko, A.V. Nikitin, J. Orphal, V.I. Perevalov, A. Perrin, A. Predoi-Cross, C.P. Rinsland, M. Rotger, M. Simeckova, M.A.H. Smith, K. Sung, S.A. Tashkun, J. Tennyson, R.A. Toth, A.C. Vandaele, J. Vander Auwera, *J. Quant. Spectrosc. Radiat. Transfer* **110**, 533 (2009)